

Araştırma Makalesi / Research Article

Investigation of Wear Behaviour of TiO₂ and Al₂O₃ Reinforced YSZ Coating

Ali AVCI^{1*}, Muhammet KARABAŞ²

^{1*} Hakkari University, Faculty of Engineering, Hakkari, Türkiye,

ORCID ID: <https://orcid.org/0000-0003-3901-6248>, aliavci@hakkari.edu.tr

² Kırklareli University, Faculty of Aeronautics and Astronautics of Science, Kırklareli, Türkiye,

ORCID ID: <https://orcid.org/0000-0002-0666-6132>, mkarabas@klu.edu.tr

Geliş/ Received: 15.04.2024;

Revize/Revised: 30.05.2024

Kabul / Accepted: 03.06.2024

ABSTRACT: In this study, three different ceramic powders used as thermal barriers were coated on AISI304 stainless steel by the atmospheric plasma spray method. A pin-on-disc apparatus was utilised to investigate the wear characteristics of the coatings. The effect of wear behavior of the addition of Al₂O₃ and titanium dioxide (TiO₂) into the YSZ coating was investigated. Before the wear test, sanding and polishing processes were carried out to ensure that the average surface roughness of the coatings was less than 0.8 µm. The wear test according to ASTM G99-04, was conducted on a pin-on-disc device at a speed of 143 rpm. The test was performed in a dry condition, with a minimum of 8000 cycles. The wear test utilised a 4N load and 6 mm-diameter Al₂O₃ balls. The surface properties and wear characteristics of the coatings were analysed using a scanning electron microscope (SEM) and energy-dispersive X-ray spectroscopy (EDS) after conducting coating and wear tests. The wear rate of the samples was assessed using optical profilometry. A micro Vickers test equipment was employed to assess the microhardness of the materials. The findings demonstrated that the inclusion of Al₂O₃ in YSZ led to an enhancement in wear resistance, but the incorporation of TiO₂ resulted in a notable reduction in wear resistance.

Keywords: Wear, Ceramic coatings, YSZ coating, Hardness.

1. INTRODUCTION

Ceramic materials provide many advantages when coated on metal or plastic due to their properties such as high hardness, high thermal-corrosion resistance, and low specific gravity. The coatings produced have the potential to be used in many different areas due to their superior properties such as high hardness, low density, high melting point, low thermal conductivity, and oxidation resistance, for example; microelectronics, automotive, and wear parts (Thakare et al., 2021),(Özçelik et al., 2024). These coatings are utilised for safeguarding gas turbines and engine components that

*Sorumlu yazar / Corresponding author: aliavci@hakkari.edu.tr

Bu makaleye atıf yapmak için /To cite this article

are subjected to high temperatures, particularly zirconium, because of their exceptional thermal insulating properties, high density, strong resistance to abrasion, and low thermal conductivity. In particular, gas turbines subjected to elevated temperatures utilise gearbox components, turbine blades, rocket nozzles, exhaust systems, bearings, and rings. Similarly, internal combustion engines employ piston cylinder heads, valves, internal combustion chambers, and exhaust systems (Noroozpour and Akbari, 2023),(Iqbal et al., 2024). Ceramic coating enhances engine efficiency, prolongs engine lifespan, and diminishes fuel consumption and petrol emissions (Avci et al., 2018). Thermal barrier coatings (TBC) typically include two distinct layers: a metallic bond layer and a ceramic layer. The metal bond layer treated the thermal expansion disparities between the metal material and the ceramic. A ceramic layer is a thermally insulated layer that is subjected to heat and often coated using the APS process. The significant porosity of APS coatings enables the movement of oxygen from the upper layer to the lower layer, resulting in the formation of a thermal-growing oxide between the bond layer and the ceramic layer. As temperatures grow, the generation of TGO also increases, which might result in damage. To enhance the durability of coatings and enhance their strength, it is necessary to regulate the level of porosity, optimise coating parameters, employ laser modification techniques, and utilise a suitable micro structure. Yttria stabilized zirconium (YSZ), which is stabilised with 8% wt. of yttrium, is commonly utilised as a ceramic layer material in TBC systems due to its exceptional resilience to thermal shock and oxidation, corrosion, high thermal insulating capacity, and low thermal conductivity (Avci et al., 2023). Nevertheless, the coating experiences an expansion in volume due to the phase change of YSZ coatings taking place at temperatures over 1200 °C (Jun et al., 2023). These powders enhance the resistance of calcium-magnesium-aluminosilicate (CMAS) to corrosion caused by temperature and decrease structural damage resulting from phase change at higher temperatures. Hot corrosion occurs due to chemical reactions between foreign chemicals, such as vanadium pentoxide and sodium sulfate, present in gas turbine fuel, and the stabiliser phase of ZrO_2 (Javadi Sigaroodi et al., 2024). During operation, gas turbines may come into contact with airborne particles that contain compounds of calcium, magnesium, aluminium, and silicon. When these particles make contact with high-temperature components like the wings and blades of the engine turbine, they adhere to the surfaces and lead to corrosion (Han et al., 2022), (Guo et al., 2024). Researchers are always researching ways to enhance materials and coatings in order to minimize the impact of CMAS corrosion and prolong the lifespan of turbine engines. In order to mitigate the influence of corrosion, TiO_2 and Al_2O_3 powders are incorporated into YSZ to enhance its volume, and cover any faults, cracks, and porosities that may arise during manufacture. Wang et al. (Wang et al., 2022) reported that the YSZ was mixed with 80% Al_2O_3 and 20% TiO_2 powder by weight in a mechanical mixer at a molar mass ratio of 1:3. Subsequently, an isothermal oxidation test was conducted on both the traditional TBCs and the Al_2O_3 - TiO_2 composite coating. A morphological and hardness examination was performed to assess the properties of the samples. The addition of Al_2O_3 in the coatings resulted in a higher level of resistance in comparison to traditional TBCs. The interaction between TiO_2 and liquid CMAS is responsible for this development, as it aids in the concentration process of CMAS. Yuan et al. (Yuan et al., 2021) manufactured ceramic powders and formed plates using various compositions of Al_2O_3 and TiO_2 , together referred to as ATYSZ. The findings demonstrated that the addition of 10% mol Al_2O_3 and 5% mol TiO_2 (10A5TYSZ) to YSZ resulted in a material that effectively endured CMAS corrosion and had suitable thermal conductivity.

The plasma spray technique yields coatings that exhibit favorable tribological properties and exceptional resistance to wear. The wear and friction characteristics of plasma spray ceramic coatings are primarily influenced by the coating's composition and microstructural properties, including

porosity, morphology, microcracks, and distribution. Based on current literature, the tribological performance of YSZ coatings is influenced by several factors such as different contaminants, dust formations, and operational conditions, including applied loads and wear rates. Various techniques can be employed to prevent metal surfaces from experiencing leakage, including mechanical, chemical, electrochemical, or laser modification methods (Critchlow and Brewis, 1996). Lima and Marple (Lima and Marple, 2005) incorporated TiO_2 into Al_2O_3 using the high-velocity oxygen and fuel (HVOF) technique. The HVOF must be applied through spraying and have to demonstrate exceptional resistance to wear and hardness. Bai et al. (Bai et al., 2023) investigated the abrasion resistance of YSZ coatings over a temperature range of 25 to 800 °C. In addition, the wear and tear of the equipment was exacerbated by the increasing temperatures. Nevertheless, the tribolayer, which is facilitated by the creation of alumina tracks on the surface, provides protection against wear at temperatures exceeding 200 °C. Ormancı et al. (Ormancı et al., 2014) examined the fracture strength and stiffness properties by incorporating both YSZ and TiO_2 into Al_2O_3 . The researchers discovered that Al_2O_3 -YSZ compounds exhibit greater hardness compared to monolithic Al_2O_3 . Furthermore, they observed that the hardness of these compounds diminishes as the YSZ content increases. In order to investigate the effects of wear on TBCs in the workplace, three distinct thermal barriers were coated using atmospheric plasma techniques. These barriers included YSZ, YA, and YAT. A wear test was conducted utilising the pin-on-disk method to investigate the wear characteristics of the coatings under dry conditions. The deformation features and microstructure were investigated using electron microscopy and EDS analysis.

2. MATERIALS AND METHODS

2.1 Materials

The investigation involved the use of AISI 304 austenitic stainless steel (SS) substrate materials, which were precisely cut into circular shapes with a diameter of 1 inch using a laser technique. To improve the mechanical adhesion of the bonding layer, the surfaces of SS coupons were abraded using alumina a fine abrasive material called 200 grit alumina was applied. The alumina particles were abraded from a distance of 30 cm at an angle of approximately 90°, and the spraying process lasted for at least 1 minute. Figure 1a) depicts a three-dimensional representation of the surface smoothness of SS following the process of sanding. The 3D pictures were quantified using the Veeco WYKO NT1100 optical profilometer, resulting in a notable enhancement in smoothness following the sanding process. The substrate material exhibited a Ra value of 358.68 nm in terms of surface roughness, while the grit-blasted substrate material showed a Ra value of 2.69 µm.

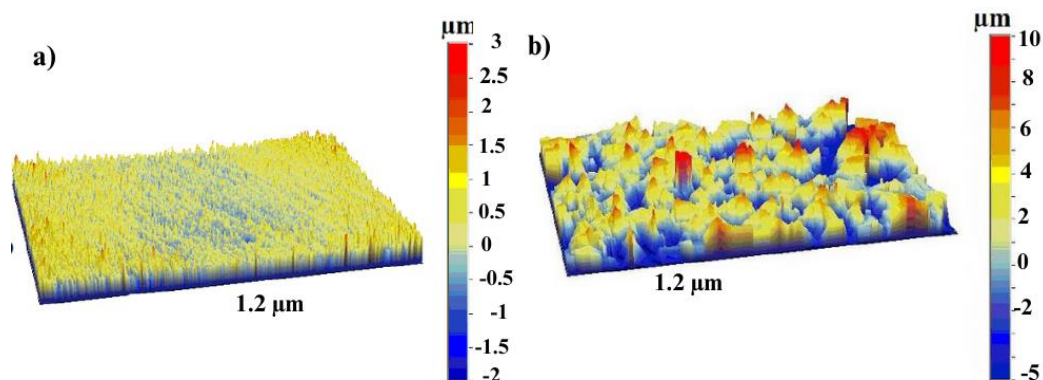


Figure 1. Surface roughness of a) AISI304 before grit blasting, b) AISI304 after grit blasting (Bal et al., 2018)

In the production of TBCs, Sulzer Metco AMDRY 997 (Ni 23Co 20Cr 8.5Al 4Ta 0.6Y) is used for the production of bond layer coatings, and YSZ 204B-NS, commercially offered by Sulzer Metco, is used for the production of ceramic top layer coatings, Al₂O₃ with a purity rate of 98.0%. Metco 105 NS White and TiO₂ powders were used. Figure 2 shows SEM images of the powders. The mixing ratios of the composite composites produced are given in Table 1.

Table 1. Chemical composition of the deposited coating

Sample Name	Feedstock powders		
	YSZ	Al ₂ O ₃	TiO ₂
YSZ	100	-	-
YA	83	17	-
YAT	80	17	3

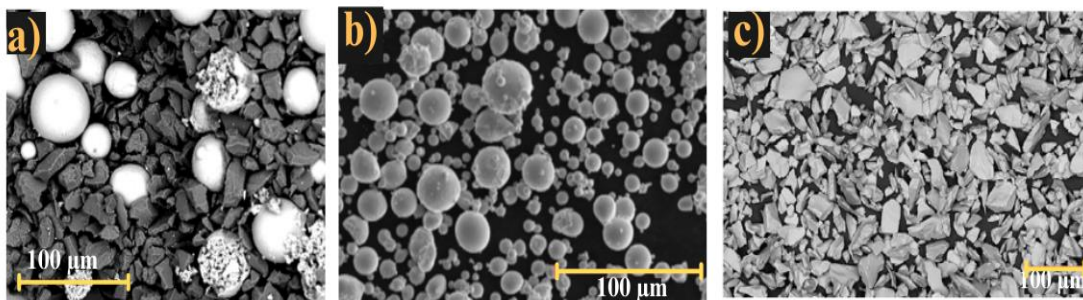


Figure 2. Microstructure of deposited powders; a) Al₂O₃ /YSZ and b) AMDRY 997 bond coat c) TiO₂

A three-axis CNC table supported a Metco DJ2700 HVOF gun that runs at a 200 mm/min. The nozzle utilized in the coating procedure was positioned along the central axis of the 3-axis CNC machine, and the mobile nozzle facilitated the uniform coating of the samples on the revolving table. The coupling layer is coated using the HVOF process, and the parameters specified in Table 2 are maintained at a constant value. Within this method, precise control over the gun's movement and the speed of the samples allows for the attainment of coatings with the necessary thicknesses. The energy was derived from the combustion of the air-propane gas mixture with oxygen. In order to achieve the requisite bond layer thickness of $85 \pm 15 \mu\text{m}$ using the HVOF approach, the metal subsurface was coated with 12 passes.

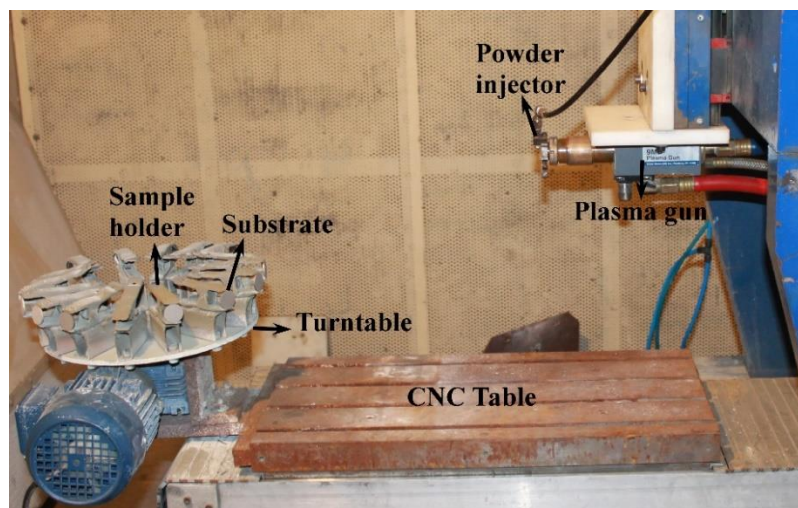


Figure 3. Schematic view of the APS system

Table 2. HVOF deposition parameters

Material	Pressure (Bar)			Flow rate (SCFH)			Process parameters		
	Oxygen	Propane	Air	Oxygen	Propane	Air	Spray distance (mm)	Feeding speed (g/s)	Spray angle (°)
Amdry 997 (Ni23Co20Cr8.5Al4Ta 0.6Y)	10.3	6.2	7.2	24	40	50	250	50	90

Ceramic top layer coatings are produced by atmospheric plasma spraying (APS). The primary and secondary gases and production parameters used in the APS method are shown in Table 3. Before coating, YSZ, alumina, and TiO₂ composite powders were mixed in alcohol for 4 hours in a mixer (turbula). The dried ceramic powders were successfully coated by plasma spraying method using Sulzer Metco 9 MBM plasma spray gun.

Table 3. APS deposition parameters

Parameters							
Current (A)	Primary Gas, Ar(scfh)	Secondary Gas, H ₂ (scfh)	Carrier Gas, Ar(scfh)	Spray Distance (mm)	Gun Speed (mm/s)	Rotation Speed (Hz) rpm	Voltage (V)
500	90	15	13.5	75	200	40	60

2.2 Microstructural Characterization

The surface and cuts of the produced coatings were examined with an electron microscope. For this purpose, the coatings were primarily subjected to metallographic grinding and polishing. For the examination of the cuts, the coatings were cut with a diamond cutter and then mowed and metallographic polishing. The microstructure tests of the samples were carried out with the optional EDS Phenom XL SEM device in different sizes. The worn tracks were examined with an optical microscope and SEM as well. In SEM studies, different detectors were used to understand the characteristics of the type of wear. EDS analyses were carried out using the mapping method for wear tracks.

2.3 Wear and Microhardness

The state of the surface is the primary determinant of the tribological performance of the coatings. The samples' surface smoothness after coating ranges from 1.5 to 2.4 μm . The melting and polishing procedures were performed to achieve an average surface roughness (Ra) of less than 0.8 μm for the coatings. The surface roughness was quantified by taking measurements at a minimum of five distinct locations on the surface, using a radius of 5 μm . Next, the sample surfaces are thoroughly cleansed using acetone to remove any oils or undesired debris and then dried using hot air. The weight of the coatings has been measured both before and after wear using a precise track in order to determine the amount of wear loss. The displacement test for each sample was conducted using a pin-on-disk device (Tribo Tester, France) operating at a speed of 143 revolutions per minute (rpm) and a minimum of 8000 cycles in a dry environment, following the guidelines of ASTM G99-04. The wear test utilised 6 mm diameter Al₂O₃ balls under a fixed load of 4N. The thickness of the traces produced during the wear test was measured using an optic microscope in order to estimate the amount of deformation.

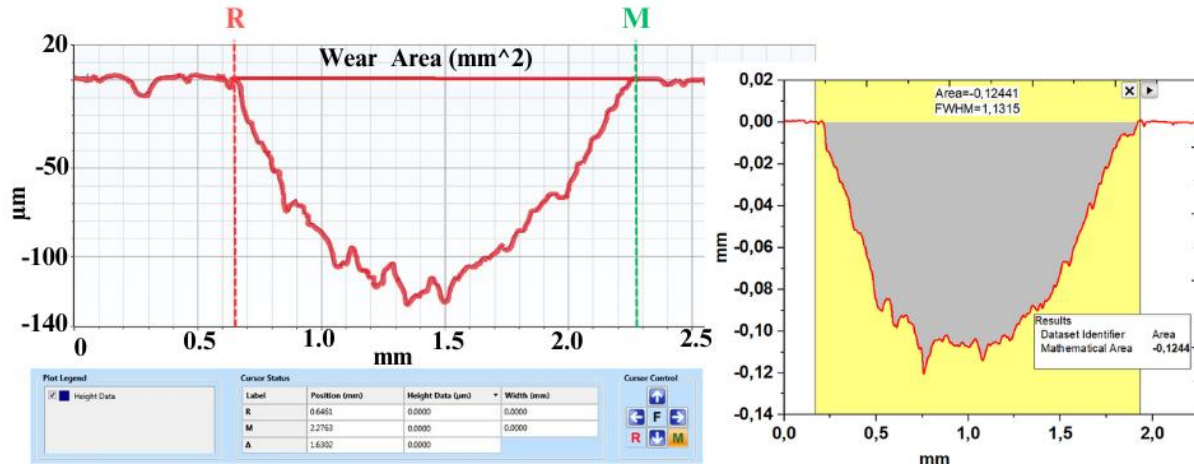


Figure 4. Wear volume measurement

Figure 4 shows the 2D profile of the wear trace taken from the mechanical profilometer. For area calculation, the area of the curve was redrawn with the help of Origin Lab Pro software, and the amount of wear was found with the help of the formulas below.

$$\text{Equation:1 Volumetric wear rate } \frac{\text{mm}^3}{\text{Nm}} = \frac{\text{Volume loss (mm}^3\text{)}}{\text{Sliding Distance (m)} \times \text{Applied load (N)}}$$

The volumetric wear rate was calculated from Equation 1 (Franco et al., 2024). The friction coefficient was provided directly by the wear tester device. The wear volume was calculated with the help of a profilometer as seen in Figure 4. In this study, the sliding distance was used as 250 m and the applied load was 4 N for each sample. Since there is no obvious wear on the alumina abrasive ball; the wear of the alumina ball is ignored in calculations.

The coatings produced in the atmospheric plasma spraying technology get increasingly tougher as the spraying speed increases. The presence of oxides in the coating often enhances its hardness while reducing its adhesive strength. The hardness of the coating layers fluctuates based on factors such as porosity, the heterogeneous structure of the layer, and the applied stress values. The hardness measurements were obtained from the surface of the coatings using the HVS1000 micro-vickers, manufactured by Bulut Machine in Türkiye. The charging duration for a mass of 300 grams is established as 15 seconds. The outcome was obtained by calculating the arithmetic mean of 10 hardness values that were randomly tested at 12 distinct points on the surface of the sample. The highest and smallest measurement values were disregarded in this calculation. The measurement was conducted with a minimum distance of 3 mm from the edges to prevent errors that could lead to the building of tension on the edges and an uneven distribution of the applied load when the floating end comes into contact with the sample. The surface roughness has been evaluated at a Ra below 0.8 µm due to its impact on the mechanical characteristics of the material.

3. RESULTS AND DISCUSSION

3.1 Microstructural characterization

Figure 5 shows micro-SEM images of coatings deposited by the APS process. Figure 5a shows a cross-sectional SEM image of YSZ coating. Upon examination of the cross-sectional SEM image, it was found that there was a ceramic top layer measuring roughly 135 µm and a bond layer measuring 75 µm. The YSZ exhibits a laminar structure and contains some voids. Figure 5b presents a cross-sectional of the YA coating. Deposition of lamellar alumina and YSZ plates has been achieved

effectively. The dark regions depicted in the image correspond to alumina, whilst the white regions correspond to YSZ. Figure 5c displays the cross-section and specific features of the YAT coating. The grayscale in the microstructure of the plates are attributed to TiO_2 . Additionally, the slices exhibited both porosity and inter-splat crackles. These structures are all created by the inherent properties of the APS coating in TBCs. Porosities are formed from the consecutive deposition of unmelted or partially melted particles during the coating process. Intersplat crackles are created through a process of cooling and collision, where hot particles pass through a plasma flame and gather as splats upon impact with a surface. In thermal barrier applications, the presence of porosity and interplate fissures hinders the transport of phonons. This diminishes the layer's heat conductivity. Porosity in TBC applications can reach a maximum of 20%. Coatings with a porosity exceeding this amount exhibit reduced adhesion and cohesiveness. During the investigation of porosity using image analysis, it was found that the YSZ coating has a porosity level of around 15%, while the YAT coating has a porosity level of 4.5% and the YAT coating has a porosity level of 3.8%. The presence of Al_2O_3 and TiO_2 in YSZ greatly decreased the porosity rate of the coated layer (Özçelik et al., 2024). The combination of Al_2O_3 (2000 °C) and TiO_2 (1850 °C) powders, which have a lower erosion point, led to the development of a denser layer of splats during plasma spraying compared to YSZ (2700 °C). The thickness of the binding layer is $85 \pm 15 \mu\text{m}$. The addition of alumina and TiO_2 to YSZ resulted in a reduction in porosity of around 65% and 70% respectively.

In Figure 5d, the surface SEM of the YSZ coating shows spaces with semi-melted or non-melted particles. The areas shown as black in Figure 5e belong to alumina, whereas the areas seen as YSZ are white. Similar microstructural defects were observed in Figure 5f above.

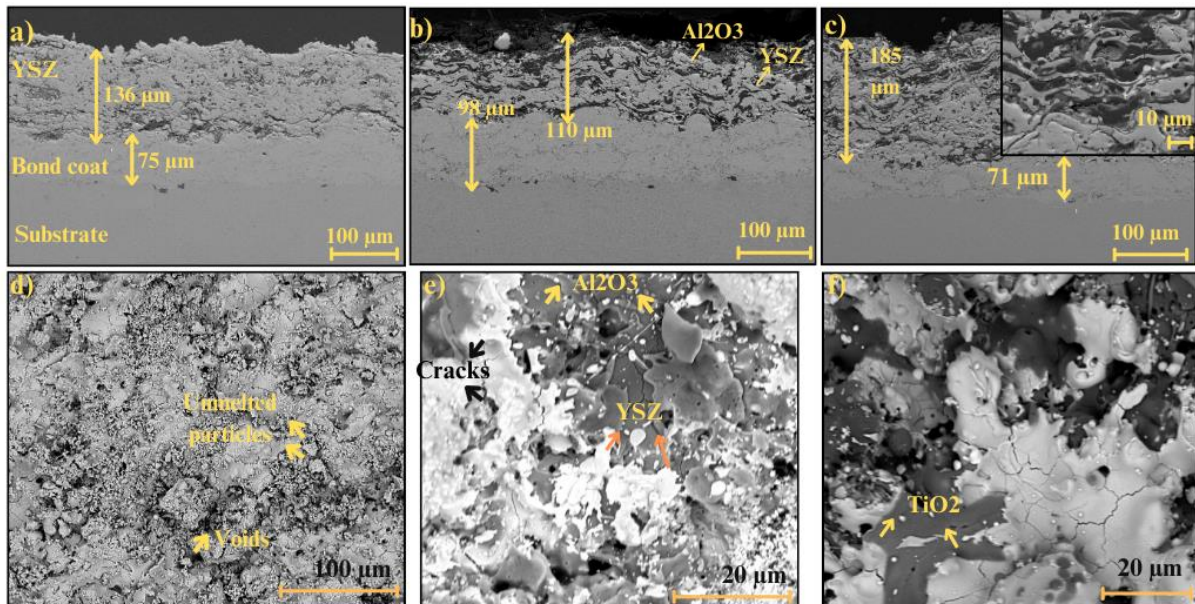


Figure 5. SEM images of coatings; a) Cross-sectional SEM image YSZ, b) Cross-sectional SEM image YA, c) Cross-sectional SEM image YAT, d) Surface SEM image YSZ, e) Surface SEM image YA, e) Surface SEM image YAT

3.2 Hardness and wear behavior of coatings

The impact of incorporating Al_2O_3 and TiO_2 particles into YSZ on the mechanical characteristics of the composite coating was assessed by a hardness test and a wear test. Figure 6a displays a graph that shows the hardness test results of the coatings. The SS substrate was determined to have the lowest hardness value. The YSZ coating exhibited a hardness of $1030 \pm 30 \text{ HV}$, which was

enhanced by roughly 25% to 1294 ± 34 HV upon the incorporation of 10% alumina particles. Nevertheless, it was discovered that the inclusion of the TiO_2 addition had a substantial impact on the hardness of the material, causing structural damage. The impact of adding TiO_2 to YSZ on its hardness is typically influenced by the composition, microstructure, and treatment factors. Wang et al. (Wang et al., 2024) reported that the microhardness and porosity of Al_2O_3 -13 wt% TiO_2 coating are 856.6HV0.5 and 12.77 %, respectively. When the porosity of the coating decreased to around 8.21%, the hardness value increased and became 1061.4HV(0.5). This is a similar example of how decreasing porosity increases hardness. However, in general, the addition of TiO_2 into YSZ matrix can increase the mechanical properties. This increase can often manifest itself in properties such as fracture, fracture toughness, and wear resistance. The variation in material characteristics is likely due to the essential role played by the quantity of TiO_2 incorporated into the YSZ. Elevated quantities of TiO_2 typically lead to an augmentation in hardness. Moreover, the mechanical properties of the material are determined by the distribution and crystalline structure of TiO_2 within the YSZ. Probably, the reduced TiO_2 concentration resulted in a decrease in the hardness measurement. The enhancement of microcirculation is a result of dispersion. When a good dispersion is achieved, the hardness and mechanical characteristics of TiO_2 particles, which hinder plastic deformation, will increase (He et al., 2022). When the cross-sectional SEM images are examined in Fig. 5c, the distribution of TiO_2 is largely understood. However, due to the nature of the APS technique, agglomeration during flow and voids in the microstructure reduced the hardness value. The higher alumina particle size and being more compatible with YSZ increased the hardness. The hardness value of SS material was found to be 216 ± 19 HV. This value is compatible with the austenitic stainless steel mentioned in the literature (Zhao et al., 2005). TiO_2 is utilised for its ability to enhance the resistance of TBCs against calcium-magnesium-aluminosilicate (CaO - MgO - Al_2O_3 - SiO_2) and hot corrosion. Wang et al. (Wang et al., 2022) conducted a study where they combined YSZ with 80% Al_2O_3 and 20% TiO_2 powder by weight to create a composite coating. The YSZ hardness value of the composite coating was initially measured at 920 HV. However, the inclusion of TiO_2 resulted in a reduction of this value to 577 HV. Nevertheless, the presence of the thermal barrier enhanced the coating's resistance to CMAS and thermal shock by facilitating the transformation from t- ZrO_2 to m- ZrO_2 . Shen et al. (Shen et al., 2019) investigated the impact of TiO_2 and samarium-added serum oxide (SDC) supplementation on the characteristics of YSZ electrolytes. The hardness results are highly similar. Luo et al. (Luo et al., 2019) investigated the microstructure and the impact of TiO_2 concentration on the mechanical and wear characteristics of YSZ ceramics produced using pressure-free sintering. It was discovered that the YSZ ceramics seen a drop in micro-hardness and wear resistance as the TiO_2 level rose. The researchers discovered that the TiO_2 ratio that induced the highest level of sleepiness was 5%. Yuan et al. (Yuan et al., 2021) utilised the APS approach to coating YSZ with Al_2O_3 and TiO_2 particles at various concentrations. They next examined the impact of CMAS corrosion on the mechanical characteristics. The addition of Al_2O_3 and TiO_2 composite coatings has resulted in an increase in the CMAS resistance and hardness levels. According to the literature, adding TiO_2 in amounts less than 5% does not consistently lead to the required enhancement in mechanical characteristics. On the other hand, TBCs enhance the expected resistance to thermal shock and CMAS. The method of manufacture and the porosity rate of the coating have a substantial impact on this condition. In our previous study, the hardness of the nano YSZ coating created using the electrophoretic deposition technique was measured to be 729 ± 78.6 HV. However, when we introduced TiO_2 in the nanoscale, the hardness decreased to 714.2 ± 92.3 HV.

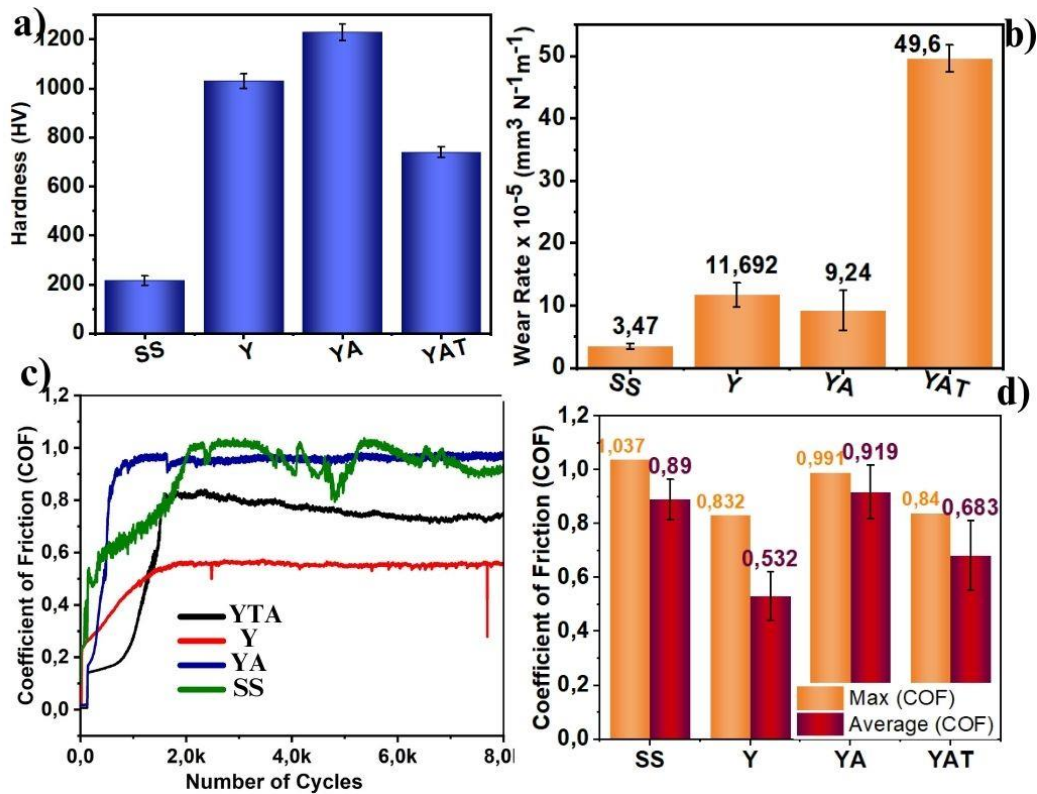


Figure 6. a) Hardness values, b) Wear rate, c), d) Coefficient of friction of coatings and SS

Figure 6b shows the rates at which the coatings and substrate experience wear and tear when subjected to a load of 4N. The distortion rates were derived from Archard's equation. A profilometer was employed to ascertain the magnitude of the displacement's volume. Based on these findings, the YAT sample exhibited the most significant wear, measuring around $50 \times 10^{-5} \text{mm}^3 \text{N}^{-1} \text{m}^{-1}$. The YSZ coating exhibits a wear resistance of $11.6 \times 10^{-5} \text{mm}^3 \text{N}^{-1} \text{m}^{-1}$, whereas alumina has a lower wear rate. The reduction in the porosity rate had a notable impact when a denser microstructure was achieved. Franco et al. discovered that as the porosity of the YSZ coating decreased, the resistance to wear rose (Franco et al., 2024). The inclusion of alumina resulted in a notable 26% enhancement in the wear resistance of YSZ, but the addition of TiO_2 had a considerable detrimental effect on its wear resistance. The friction ratio and hardness values of the coatings exhibited a direct correlation with the degree of wear. Coatings that exhibit a lower average friction rate also demonstrate a correspondingly lower wear rate. Furthermore, the presence of the newly formed $\text{Al}_{0.1}\text{Zr}_{0.9}\text{O}_{1.95}$ (Chen et al., 2018) phase has significantly enhanced the durability of the coating. Enhanced toughness can also enhance the coating's resistance to wear. The friction coefficients are provided in Figures 6c and 6d, based on the number of cycles of the sub-material and the coatings. The friction coefficients acquired from the wear test equipment during the abrasion test are provided in Figure 6c. It was observed that the friction coefficient of the SS substrate material fluctuated under 4 N load and 60 mm s^{-1} speed conditions. The coefficient of friction (COF) exhibited a fluctuating pattern and gradually rose until the 2000th cycle. However, after the 2000th cycle, it reached a stable value of the 3500th cycle. The mean COF value was 0.89 ± 0.075 . The coefficient of friction (COF) of the $\text{Al}_2\text{O}_3/\text{TiO}_2$ coating reduced as the YSZ percentage increased. In Mehar's study (Mehar and Sapate, 2024) similar results were obtained, with the YSZ coating exhibiting the lowest friction coefficient. The probable reason for this variation is the exhaustion of metallic components, as seen by the visible signs of erosion in Figure 7. Additionally, it is recognised that the SS substrate, which has an

austenitic structure, undergoes a partial martensitic transformation when subjected to a load. This transformation leads to an increase in its hardness (Özçelik et al., 2024). In this instance, it results in an increase in the COF value (Zandrahimi et al., 2007). Upon examination of the YSZ COF chart, it was found that the average coefficient of friction was 0.53 ± 0.09 . Additionally, the curve showed a steady progression towards the end, which occurred after about 2000th cycles. The average coefficient of friction between the YSZ and Al_2O_3 values rose from 0.53 ± 0.09 to 0.91 ± 0.01 . The coefficient of friction increased due to the presence of hard alumina particles surrounding the ZrO_2 particles, similar to the findings of microhardness tests. The YAT sample exhibited an average friction coefficient of 0.68 ± 0.13 . The addition of an extra 3% TiO_2 by weight resulted in a fall in hardness and a reduction in wear resistance. Like other coatings, the graphic in the YAT sample started to become less raised around the end of the 2000 cycle. However, in contrast to others, the rate of friction decreased.

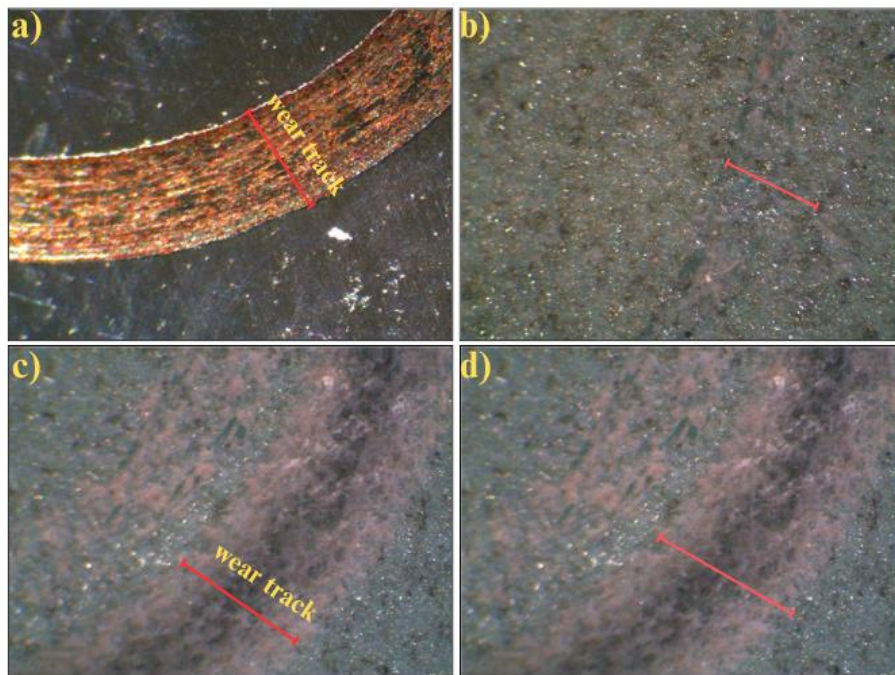


Figure 7. AISI, YSZ, YA, YTA Microscopic image of the marks formed after the wear test; a) SS, b) YSZ coating, c) YA, and d) YTA

Figure 7 shows optical microscopic images of the traces that were created following the wear test. The ceramic coatings exhibit wear marks and profiles that are distributed across the surface, whereas the metal substrate leaves behind a single mark. The size of the SS sample was 0.75 ± 0.0075 mm, whereas the ceramic coatings had measurements of YSZ 0.86 ± 0.46 mm, YA 1.072 ± 0.13 mm, and YTA 1.71 ± 0.05 mm, respectively. Figure 8 depicts the microscopic structure of the coatings that have undergone wear. The SEM images display accurate wear surfaces, instances of pull-out defects, and wear debris. Additionally, it has been noted that ceramic coatings exhibit indications of wear that result from several wear mechanisms. The SEM picture of SS is depicted in Figure 8 a,e. The AISI 304 surface underwent scratching, leading to the production of straight grooves and plastic deformation. Despite the low surface hardness, ceramics exhibit superior wear resistance compared to SS because of two primary factors. The first transformation is the conversion of the austenitic phase into martensite under load, as previously mentioned in the hardness section. Furthermore, the SEM photos clearly demonstrate that the folding of the metal leads to an enhanced surface flatness following a certain circuit. Upon examining the coated surface, it was seen that the presence of rigid,

abrasive particles or a higher level of hardness on the top surface compared to the lower layer could result in abrasive phenomena. The presence of solid corrosive particles is a result of the transformation of austenite and the creation of martensite residues during the wear test (Zandrahimi et al., 2007). For both coatings, ductile wear, deformation wear and brittle deformation, and finally ductile deformation wear mechanisms were observed for ceramic coatings. These wear types have been reported for YSZ and YA (Franco et al., 2021, 2019). Figure 9a displays the outcomes of the mapping EDS examination conducted on the surface of the SS sample. The EDS analysis revealed the existence of oxygen.

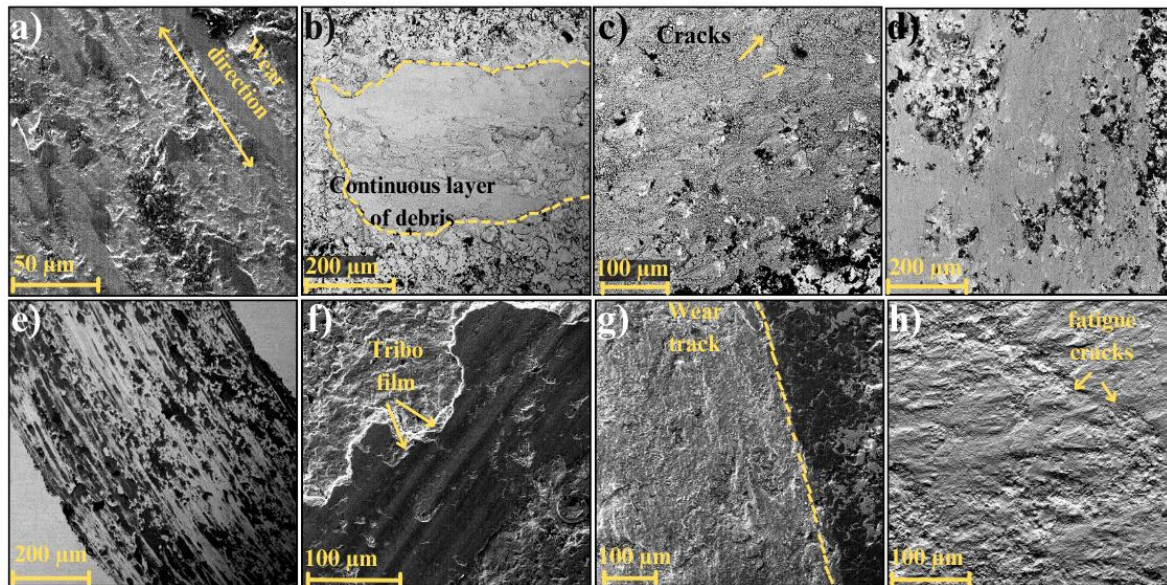


Figure 8. SEM images of wear tracks; a),e) SS, b),f) YSZ coating, c),g) YA coating, and d),h) YAT coating

Figure 8b, f displays evidence of erosion on the YSZ coating. Tribofilm formation may occur in the trace of dislocation. This phenomenon arises when the worn coating powder is retained on the surface due to the applied load. The SEM pictures revealed the presence of worn grooves. At the conclusion of each circuit of the bullet, various types of creases are created. Figure 9b shows the EDS examination of the YSZ worn surface, which revealed the presence of acceptable levels of take and oxygen elements. Adhesive wear was identified as the specific type of wear in this case. Adhesive wear is a type of wear that occurs when materials make contact and rub against each other. Due to this friction, the atoms on the surfaces of the materials interpenetrate, resulting in surface damage to the material. The SEM image data for the YA sample is represented in Figure 8 c, g. The SEM images acquired indicated the presence of microcracks. The cracks originated from fatigue caused by repeated use. The presence of micrometer-sized imperfections, such as fractures in the mechanism and splinters in the coatings, could potentially be the cause of the cracking. The EDS analysis results of the YA sample reveal the presence of Al and O elements, as depicted in Figure 9c. Both the deceiver and the flock possess the presence of Al and O. However, SEM images showed that the coating was in the correct direction. This can be explained by abrasion in case of abrasion, that is, the wear of surfaces without contact with hard diseases or other hard surfaces that can damage their surface. SEM images of the YTA sample are given in Figure 8 d,h. In the EDS results of the YAT sample in Figure 9d, it was understood that the black areas where corrosion was allowed were alumina.

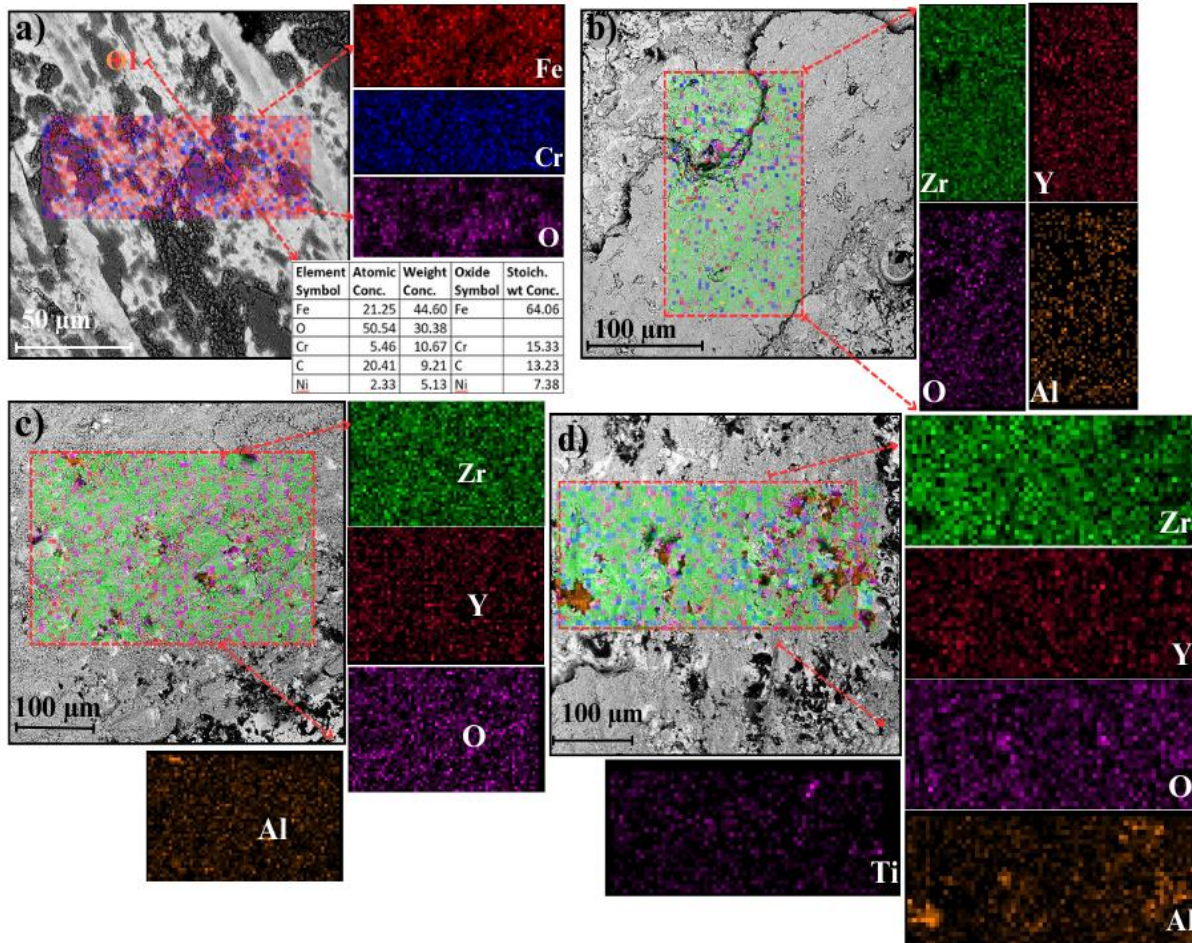


Figure 9. EDS mapping results a) SS, b) YSZ coating, c) YA coating, and d) YAT of samples after wear tests

4. CONCLUSION

The investigation involved applying atmospheric plasma spray to an SS substrate in order to coat it with composite TBCs. These coatings included YSZ, YA, and YAT. A pin-on-disc tribological test was conducted to investigate the wear characteristics of the coatings. The acquired results are summarized below:

-The inclusion of Al_2O_3 in YSZ resulted in a 25% increase in microhardness. Nevertheless, the additional TiO_2 resulted in a reduction in hardness.

-As the discharge rate increases, the wear rate of the samples decreases. The YAT sample has the highest wear rate.

-The YSZ sample exhibited abrasive adhesive wear upon the introduction of Al_2O_3 .

-By incorporating alumina and TiO_2 into YSZ, the porosity was reduced by roughly 65% and 70% respectively.

5. ACKNOWLEDGEMENTS

The authors thank Dr. Emre BAL and Dr. Ayşegül ADOĞAN EKER for their wear test contributions.

6. CONFLICT OF INTEREST

Author(s) approve that to the best of their knowledge, there is not any conflict of interest or common interest with an institution/organization or a person that may affect the review process of the paper.

7. AUTHOR CONTRIBUTION

Ali AVCI: Testing and Analyzing-Writing-original draft, Resources, Methodology, Supervision, Investigation. Muhammet KARABAŞ: Coating-Writing-original draft, Funding acquisition, Data curation.

8. REFERENCES

- Avcı A., Eker A. A., and Eker B., Exergetic, Energetic and Environmental Dimensions, Elsevier Publications, Academic Edition, Netherlands, pp. 793-814, 2018.
- Avcı A., Karabaş M., Akdoğan Eker A., Akman E., & Aslan C., Improvement of CMAS resistance of laser glazed and nano-modified YSZ thermal barrier coatings, *Ceramics International*, 50 (7), 9985-9999, 2024.
- Bai L., Zhang H., Wan S., Yi G., Sun H., Tailoring wear and tribo-induced interaction of YSZ coating sliding against Si₃N₄ and Al₂O₃ counterparts, *Wear*, 518–519 (1), 204628, 2023.
- Bal E., Karabaş M., Yılmaz Taptık İ., The effect of CMAS interaction on thermal cycle lifetime of YSZ based thermal barrier coatings, *Materials Research Express*, 5(6), 065201, 2018.
- Chen, K., Song, P., Hua, C., Zhou, Y., Huang, T., Li, C., Lu, J., Effect of YSZ-dopant on microstructure and hardness property of the Al₂O₃–40%TiO₂ plasma sprayed coating, *Materials Research Express*, 5, 086504, 2018.
- Critchlow G. W., Brewis D. M., Review of surface pretreatments for aluminium alloys. *International Journal of Adhesion and Adhesives*, 16(4), 255–275, 1996.
- Franco D., Ageorges H., López E., Vargas F., Tribological performance at high temperatures of alumina coatings applied by plasma spraying process onto a refractory material, *Surface and Coatings Technology*, 371, 276–286, 2019.
- Franco D., Ageorges H., López E., Vargas F., Wear behavior at high temperatures of ZrO₂ - Al₂O₃ plasma sprayed coatings and an electro-melted AZS refractory, *Surface and Coatings Technology*, 425, 127715, 2021.
- Franco D., Vargas F., López E., Ageorges H., Wear behavior at high temperature of ZrO₂–Y₂O₃ (YSZ) plasma-sprayed coatings, *Journal of Materials Science*, 59(1), 20–37, 2024.
- Guo L., Zhang B., Gao Y., Yan K., Interaction laws of RE₂O₃ and CMAS and rare earth selection criterions for RE-containing thermal barrier coatings against CMAS attack, *Corrosion Science*, 226, 111689, 2024.
- Han J., Zou Y., Wu D., Chen J., Zhang Y., Improving CMAS-corrosion resistance of YSZ-based thermal barrier coatings with Al₂O₃ addition, *Surface and Coatings Technology*, 446, 128799, 2022.
- He Y., Zhang S., He Y., Song R., Zhang Z., Liu B., Li H., Shang guan, J., Effects of yttrium-stabilized zirconia (different yttrium content) doping on the structure, corrosion resistance and wear resistance of Ni-P electroless coating, *Colloids and Surfaces A: Physicochemical and Engineering Aspects*, 654, 130059, 2022.

- Iqbal A., Moskal G., Cavaleiro A., Amjad A., Khan M. J., The current advancement of zirconate based dual phase system in thermal barrier coatings (TBCs): New modes of the failures: Understanding and investigations, *Alexandria Engineering Journal*, 91, 161–196, 2024.
- Javadi Sigaroodi, M., Rahimi J., Poursaeidi, E., Montakhabi F., Impact of bond coat types on calcium-magnesium-alumina-silicate and hot corrosion behavior in thermal barrier coatings, *Corrosion Science*, 227, 111742, 2024.
- Jun B., Jonsson N., Jordan E. H., Cooper R. C, CMAS deposition rate and sequence effects on cyclic life in gradient testing, *SN Applied Sciences*, 5(5), 138, 2023.
- Lima R. S., Marple B. R., Superior performance of high-velocity oxyfuel-sprayed nanostructured TiO₂ in comparison to air plasma-sprayed conventional Al₂O₃-13TiO₂, In *Journal of Thermal Spray Technology*, 14 (3397), 397–404, 2005.
- Luo P., Zhang J., You, Z., Ran X., Liu, Y., Li, S., & Li, S., Effect of TiO₂ content on the microstructure and mechanical and wear properties of yttria-stabilized zirconia ceramics prepared by pressureless sintering, *Materials Research Express*, 6(12), 125211, 2019.
- Mehar, S., Sapate, S.G., Contact severity maps for plasma sprayed YSZ modified Al₂O₃-3% TiO₂ coatings *Ceramic International*, 50(8),13003–13013, 2024.
- Noroozpour M., Akbari A., YSZ–Al₂O₃ thermal barrier nanocomposites coatings: Electrophoretic deposition and characterization, *International Journal of Applied Ceramic Technology*, 21(1) 888-899, 2024.
- Ormanci O., Akin I., Sahin F., Yucel O., Simon V., Cavalu S., Goller G., Spark plasma sintered Al₂O₃–YSZ–TiO₂ composites: Processing, characterization and in vivo evaluation, *Materials Science and Engineering: C*, 40, 16–23., 2014.
- Özçelik A., Akdoğan Eker A., Karabaş M., Avcı A., Küçükyıldırım B. O.3, Enhanced CMAS and hot corrosion degradation of YSZ thermal barrier coating with nano powders, *Surface and Coatings Technology*, 481, 130624, 2024.
- Shen C. T., Lee K. R., Hsieh Y. P., Lee S. W., Chang J. K., Jang S. C., Tseng C. J., Effects of TiO₂ and SDC addition on the properties of YSZ electrolyte, *International Journal of Hydrogen Energy*, 44(56), 29426–29431, 2019.
- Thakare J. G., Pandey C., Mahapatra M. M., Mulik R. S., Thakare, J. G., Pandey, C., Mahapatra, M. M., & Mulik, R. S., Thermal Barrier Coatings—A State of the Art Review, *MMI*, 27(7), 1947–1968,2021.
- Wang, C., Liu, M., Wang, H., Jin, G., Ma, G., Zhang, J., Chen, S., Tribological properties and solid particle erosion wear behavior of Al₂O₃-13 wt% TiO₂/Al₂O₃-PF composite coatings prepared on resin matrix by supersonic plasma spraying, *Ceramic International*, 50(4), 2024.
- Wang Z., Zhang J., Han S., Liu J., Corrosion resistance of modified YSZ coatings subjected to CMAS attacks, *Surface Engineering*, 38(4), 393–401, 2022.
- Yuan K., Yang L., Wang Q., Zhang F., Zhu W., Zhou Y., Al₂O₃–TiO₂ Codoped Yttria-Stabilized Zirconia Thermal Barrier Coatings Resistant to Damage by Molten Calcium-Magnesium-Alumino-Silicate (CMAS) Glass, *Advanced Engineering Materials*, 23(6), 1-12, 2021.
- Zandrahimi M., bateni M. R., Poladi A., Szpunar J. A., The formation of martensite during wear of AISI 304 stainless steel, *Wear*, 263 (1–6), 674–678, 2007.
- Zhao X., Jing T. F., Gao Y. W., Qiao G. Y., Zhou, J. F., Wang W., Annealing behavior of nano-layered steel produced by heavy cold-rolling of lath martensite, *Materials Science and Engineering: A*, 397(1–2), 117–121, 2005.